

## Metal–Oxo Cluster Formation Using Ammonium and Sulfate to Differentiate M<sup>IV</sup> (Th, U, Ce) Chemistries

Ian Colliard,\* Jessica C. Brown, and May Nyman\*



Cite This: <https://doi.org/10.1021/acs.inorgchem.2c01309>



Read Online

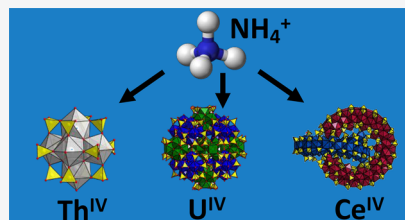
ACCESS |

Metrics & More

Article Recommendations

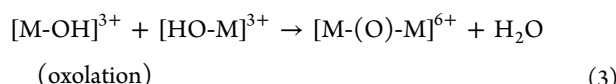
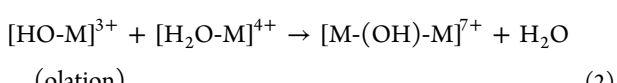
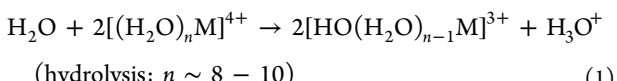
Supporting Information

**ABSTRACT:** Isolating isostructural compounds of tetravalent metals M<sup>IV</sup> (Zr, Hf, Ce, Th, U, Pu, Np) improves our understanding of metal hydrolysis and coordination behavior across the periodic table. These metals form polynuclear clusters typified by the hexamer [M<sup>IV</sup><sub>6</sub>O<sub>4</sub>(OH)<sub>4</sub>]<sup>12+</sup>. Exploiting the ammonium M<sup>IV</sup>-sulfate (Ce<sup>IV</sup>, Th<sup>IV</sup>, and U<sup>IV</sup>) phase space targeting rapid crystallization, we isolate the common hexamer [M<sup>IV</sup><sub>6</sub>(OH)<sub>4</sub>(O)<sub>4</sub>]<sup>12+</sup> but with different numbers of capping sulfates and water molecules for Ce<sup>IV</sup>, Th<sup>IV</sup>, and U<sup>IV</sup>. These phases allowed a direct comparison of bonding trends across the series. Upon cocrystallization with the hexamers, higher complex structures can be identified. Thorium features assemblies with monomer-linked hexamer chains. Uranium features assemblies with sulfate-bridged hexamers and the supramolecular assembly of 14 hexamers into the U<sub>84</sub>[U<sub>6</sub>(OH)<sub>4</sub>(O)<sub>4</sub>]<sub>14</sub>(SO<sub>4</sub>)<sub>120</sub>(H<sub>2</sub>O)<sub>42</sub>]<sup>72-</sup>. Last, cerium showcases the isolation from monomers to the Ce<sub>62</sub>[Ce<sub>62</sub>(OH)<sub>30</sub>(O)<sub>58</sub>(SO<sub>4</sub>)<sub>71</sub>(H<sub>2</sub>O)<sub>33.25</sub>]<sup>41-</sup>. Furthermore, small-angle X-ray scattering (room temperature) shows ammonium-induced cluster assembly for Ce<sup>IV</sup> but minimal reactivity for U<sup>IV</sup> and Th<sup>IV</sup>. In this study, because the phases crystallized at elevated temperature demonstrates favorable cluster assembly, these solution phase results were surprising and suggest some other characteristics such as Ce's facile redox behavior, contributes to its solution-phase speciation.



### INTRODUCTION

Tetravalent metal (M<sup>IV</sup>) cations exhibit rich polynuclear speciation in water because of their strong Broensted and Lewis acid properties. M<sup>IV</sup> metals include transition metals (Zr<sup>IV</sup> and Hf<sup>IV</sup>), lanthanides (Ce<sup>IV</sup>), and actinides (Th<sup>IV</sup>, U<sup>IV</sup>, Np<sup>IV</sup>, and Pu<sup>IV</sup>). Strategic harnessing of these aqueous M<sup>IV</sup> reactions leads to the assembly of molecular nanoclusters, inorganic frameworks, and metal–organic frameworks (MOFs) with exploitable chemistry and phenomena including catalysis,<sup>1–3</sup> nuclear waste sequestration,<sup>4</sup> biomimetic scavenging of reactive oxygen species,<sup>5</sup> and modeling environmental transport or controlled separations of actinides.<sup>6,7</sup> Moreover, the similar chemistries of these metals can be studied to understand bonding behavior across the d and f blocks of the periodic table, specifically by creating isostructural series, i.e., M<sup>IV</sup>-UiO-66 MOF structures.<sup>4,8–12</sup> Polynuclear cluster assembly is primarily influenced by the pH, buffered by both the metals and added acid or base. Excluding all other influencing factors, the self-assembly of oxo clusters proceeds by the following fundamental steps:<sup>13</sup>



While these reactions are described as a function of the pH, inner-sphere (metal–ligand) and outer-sphere (counterion) interactions can significantly alter or compete with the simple M<sup>IV</sup>-aqua reactions described above. For example, ligation can differentiate and direct aqueous phase chemistry of these metals, including the very similar Zr/Hf<sup>IV</sup>.<sup>14–17</sup> The most-readily observed species in solution and in the solid state is a hexamer; generally formulated [M<sup>IV</sup><sub>6</sub>O<sub>4</sub>(OH)<sub>4</sub>]<sup>12+</sup>. The hexamer (M<sub>6</sub>) has the same topology as the core building unit of fluorite-type M<sup>IV</sup>O<sub>2</sub>, marking the most common anchor point across the M<sup>IV</sup> cations (and the building unit for the above-mentioned UiO-66). This makes the hexamer an ideal species to study the assembly and crystallization pathways in natural and synthetic environments. Isolation of M<sub>6</sub> requires appropriate capping groups, which include acetates and amino acids (molecular clusters),<sup>18–20</sup> ditopic acetate linkers (for MOFs and coordination polymers),<sup>4,8–12</sup> or sulfates/selenates (frameworks or molecular clusters).<sup>21</sup>

**Special Issue:** Discrete Coordination Cages and Metal Clusters

Received: April 17, 2022

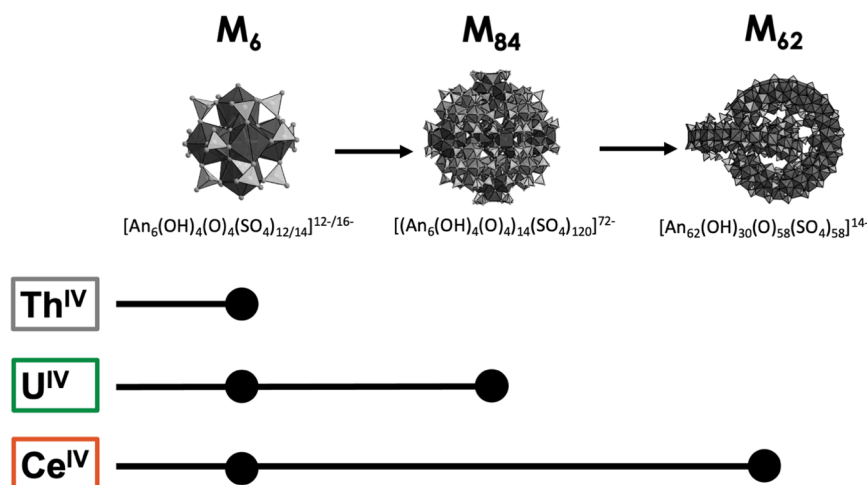


**Figure 1.** Summary and schematic of the largest metal–oxo structures isolated in this study.

Recent studies have showcased how a combination of capping ligands (i.e., sulfate) and counterions can influence the formation of different structures including M<sub>6</sub>, M<sub>84</sub> ( $M^{IV} = U$  only, “superatom” of 14 sulfate-linked U<sub>6</sub>), and M<sub>70</sub> ( $M = Zr^{IV}$ ,  $Ce^{IV}$ ,  $U^{IV}$ ; wheel of 10 hexamers fused by 10 monomers).<sup>22–24</sup> For Ce<sub>70</sub>, the use of counterions has afforded the isolation of fragments that provide insight into self-assembly mechanisms.<sup>25</sup> The different ionic behavior and hydration enthalpies for the alkali metals have been shown to influence the formation of thorium nitrato complexes and U<sub>6</sub>-sulfate lattices.<sup>26</sup>

Hard, or highly acidic, U<sup>IV</sup>, Ce<sup>IV</sup>, and Pu<sup>IV</sup> yielded larger molecular clusters, including U<sub>12</sub>, U<sub>14</sub>,<sup>27</sup> and U<sub>16</sub>,<sup>28,29</sup> Ce<sub>19</sub>, Ce<sub>22</sub>, Ce<sub>24</sub>, Ce<sub>40</sub>, and Ce<sub>100</sub>;<sup>30–33</sup> and Pu<sub>16</sub> and Pu<sub>22</sub>,<sup>7</sup> in addition to the ubiquitous hexamers; all of these resemble the parent fluorite-type oxide. Analogous M<sub>38</sub> for Ce<sup>IV</sup>,<sup>33</sup> Pu<sup>IV</sup>,<sup>34</sup> U<sup>IV</sup>,<sup>35–37</sup> and Np<sup>IV</sup>,<sup>38</sup> have been isolated, and with the exception of cerium, M<sub>38</sub> represents the largest metal–oxo clusters that contain the fluorite core. On the other hand, Th<sup>IV</sup> has not yielded any clusters larger than an octamer or a decamer (when considering oxo- and fluoro-bridged clusters), with the most common structure being the hexamer. Several intricate thorium sulfate frameworks have been isolated and structurally characterized that feature monomers, dimers, hexamers, and combinations thereof, suggesting the coexistence of these species in solution.<sup>42,43</sup>

The lack of larger thorium sulfate clusters is seemingly attributed to the “sluggish” oxidation–oxolation chemistry of Th<sup>IV</sup> because of its larger radius and softer chemistry. However, other factors could be considered including poorer solubility of assembled polynuclear species or the lack of any redox behavior (compared to redox-active Ce<sup>IV</sup>, U<sup>IV</sup>, Np<sup>IV</sup>, and Pu<sup>IV</sup>), where the redox behavior can also be harnessed to manipulate the pH and promote metal–ligand lability. In contrast to Th<sup>IV</sup>, Zr<sup>IV</sup>, Hf<sup>IV</sup>, Ce<sup>IV</sup>, Pu<sup>IV</sup>, and Np<sup>IV</sup> have yet to be isolated as well-known hexamers with sulfate capping ligands. Previous studies of Hf<sup>IV</sup>–oxo cluster formation in the ammonium sulfate “phase space” demonstrated cluster nuclearity ranging from monomers to planar hexamers to Hf<sub>11</sub> and Hf<sub>18</sub>.<sup>44–46</sup>

Prior to the current study, only Th<sub>6</sub> and U<sub>6</sub> have been isolated with sulfate. To gain further insight into the lack of larger Th<sup>IV</sup>–oxo clusters, we are targeting identical parallel synthetic environments with Th<sup>IV</sup>, U<sup>IV</sup>, and Ce<sup>IV</sup>. Counterions

such as transition metals and lanthanides (used in prior studies by us) can coordinate to sulfate ligands, highly influencing crystal formation. Ammonium thus becomes an ideal counterion because of its lack of direct structural influence of metal–oxo cluster formation, only interacting through hydrogen bonding. Strong hydrogen bonding of ammonium has also been shown to promote very rapid crystallization, i.e., for the U<sup>IV</sup>–oxo peroxide capsules.<sup>47</sup> Assured rapid crystallization via anion–cation association can circumvent uncontrolled reaction pathways due to solution aging (i.e., evaporation and absorption of atmospheric gases). Herein we report the isolation of structurally varied crystals (11 structures total) for Th<sup>IV</sup>, U<sup>IV</sup>, and Ce<sup>IV</sup> with capping sulfates and ammonium as counterions. The hexamer yet again remains a common structural anchor point, with the introduction of Ce<sub>6</sub>-sulfate (Figure 1). However, because of the polyphasic nature of the isolated crystals, new structures emerged, showcasing diverging chemistry for Th<sup>IV</sup>, U<sup>IV</sup>, and Ce<sup>IV</sup> in the ammonium sulfate reaction space. U<sup>IV</sup> and Ce<sup>IV</sup> both demonstrate the formation of larger assemblies featuring the hexamer. While U<sup>IV</sup> is limited to sulfate-linked assemblies of hexamers into chains or spheres (U<sub>84</sub>), Ce<sup>IV</sup> is isolated as Ce<sub>62</sub> (Figure 1). The M<sub>62</sub> ( $M = Ce$ ) assembly (related to M<sub>70</sub> discussed previously) differs from the M<sub>84</sub> assembly ( $M = U$ ) in that the former is the result of more extensive hydrolysis/condensation reactions, is commensurate with the slightly smaller 8-coordinate radius of Ce<sup>IV</sup> (0.97 Å) compared to U<sup>IV</sup> (1.00 Å). In addition, Ce<sup>IV</sup> is much smaller than Th<sup>IV</sup> (1.05 Å).<sup>48</sup> Furthermore, elements such as Pu<sup>IV</sup> and Np<sup>IV</sup> with comparable radii become a natural extension for similar studies on complexation and hydrolysis. As such, our study, with a focus on Th<sup>IV</sup>, U<sup>IV</sup>, and Ce<sup>IV</sup>, highlights how oxo cluster chemistry can be used to differentiate M<sup>IV</sup> chemistry for Th, U, and Ce, both from a fundamental prospective and for the development of new materials, for applications ranging from catalysis to separations, and pave the way for similar transuranic work.

## EXPERIMENTAL SECTION

**Caution!** Th and depleted U (Th<sup>232</sup> and U<sup>238</sup>, respectively) are α emitters. Standard precautions were used in the handling of radioactive materials.

**Materials.** UO<sub>2</sub>(CH<sub>3</sub>COO)<sub>2</sub>, concentrated H<sub>2</sub>SO<sub>4</sub> (98%, Macron Fine Chemicals), Th(NO<sub>3</sub>)<sub>4</sub>, Ce(SO<sub>4</sub>)<sub>2</sub> (98%, Sigma-Aldrich), and

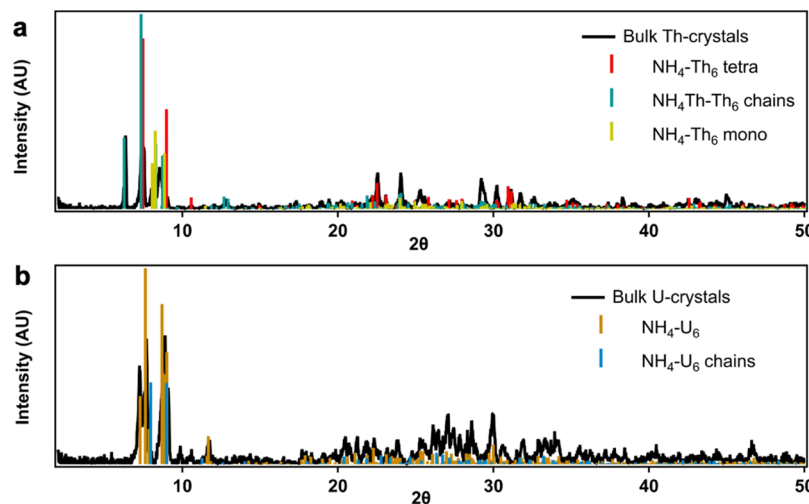


**Figure 2.** PXRD patterns for (a) thorium sulfate bulk and (b) uranium sulfate bulk, illustrating all single-crystal structures that are present in the bulk.

Millipore-filtered water with a resistance of  $18.2\text{ M}\Omega\cdot\text{cm}$  were used as received in all reactions.

**Synthesis of  $\text{U}(\text{SO}_4)_2$ .** The uranium(IV) sulfate starting material was synthesized as described previously.<sup>22</sup> Briefly, a solution of uranyl acetate in an ethanol/sulfuric acid mixture (3:1, v/v) was placed under UV light (390–400 nm, 15 W) for 24–48 h. The uranium was reduced, precipitated as uranium(IV) sulfate, and then washed. For more details, see the Supporting Information (SI).

The  $\text{NH}_4\text{-M}^{\text{IV}}$  structures were synthesized by similar methods, generally described here and detailed in the SI.  $\text{Th}(\text{NO}_3)_4$ ,  $\text{U}(\text{SO}_4)_2$ , and  $\text{Ce}(\text{SO}_4)_2$  are dissolved in 500–1000  $\mu\text{L}$  of water.  $\text{NH}_4^+$  is added as a solution of  $(\text{NH}_4)_2\text{SO}_4$  in different concentrations for each (Table S1). The screw-capped vials were then placed in a sand bath and heated for 24 h at  $75^\circ\text{C}$ . Crystalline products were isolated by filtering and washed with 0.5 M HCl, followed by water.

This experimental protocol for  $\text{Th}^{\text{IV}}$ ,  $\text{U}^{\text{IV}}$ , and  $\text{Ce}^{\text{IV}}$ , each resulting in various crystalline phases, is identified by single-crystal X-ray diffraction (SCXRD). As such, powder X-ray diffraction (PXRD) of bulk crystalline material confirmed the polyphasic crystalline material as well as the identification of all phases (Figures 2 and S1).

**Crystallographic Studies.** All crystal structure data sets were collected at 173 or 100 K on a Rigaku Oxford SynergyS diffractometer, equipped with a PhotonJet S Cu source ( $\lambda = 1.54184\text{ \AA}$ ) and a hyPix-6000HE photon counting detector at 173 or 100 K. All dataframes were collected and processed using *CrysAlis Pro*, version 171.40\_64.53 (Rigaku Oxford Diffraction, 2018).<sup>49,50,51</sup> After integration, both (analytical) absorption and empirical absorption (spherical harmonic, image scaling, and detector scaling) corrections were applied.<sup>52</sup> All structures were solved by the intrinsic phasing method from the *SHELXT*<sup>53</sup> program developed by successive difference Fourier syntheses and refined by full-matrix least squares on all  $F^2$  data using *SHELX*<sup>52</sup> via the *OLEX2* interface.<sup>53</sup> Further information on the refinement, disorder, and solvent mask can be found in the SI.

**PXRD.** Samples for PXRD were prepared by filtering and washing freshly synthesized crystals. The samples are named  $\text{NH}_4\text{Th-Bulk}$  (containing  $\text{NH}_4\text{-Th}_6$  and  $\text{NH}_4\text{Th-Th}_6$ ),  $\text{NH}_4\text{U-bulk}$  (containing  $\text{NH}_4\text{-U}_6$  and  $\text{NH}_4\text{-U}_6\text{-chains}$ ), and  $\text{NH}_4\text{Ce}(\text{SO}_4)_{5/6}$ . The Ce-monomer crystals were manually separated from the  $\text{Ce}_6$  and  $\text{Ce}_{62}$  phases. The crystals for each sample were ground in a mortar and pestle. PXRD patterns were collected from  $2\theta = 3\text{--}50^\circ$  at a rate of  $1.5^\circ\text{ min}^{-1}$  using a Rigaku Miniflex diffractometer with Cu  $\text{K}\alpha$  ( $\lambda = 1.54056\text{ \AA}$ ) and Mo  $\text{K}\alpha$  ( $\lambda = 0.70930\text{ \AA}$ ) radiation. Crystals for  $\text{NH}_4\text{-U}_{84}$  and  $\text{Ce}_{62}$  lose their crystallinity upon dehydration because of >30% disordered solvent-accessible void space within the unit cells. Several attempts to procure PXRD patterns showed amorphization upon dehydration.

**Small-Angle X-ray Scattering (SAXS).** SAXS data were collected on an Anton Parr SAXSess instrument utilizing Cu  $\text{K}\alpha$  radiation and line collimation. Data were recorded on an image plate in the range of  $0.008\text{--}2.5\text{ \AA}^{-1}$ . The sample and image plate are distanced 26.1 cm apart. Solutions were measured in 1.5 mm glass capillaries. Water was used as the background, and scattering was measured for 30 min. SAXSQUANT software was used for data collection and processing (normalization, primary beam removal, and background subtraction). All other data analyses were carried out with the IRENA macros within IGOR Pro.<sup>54</sup> Simulated scattering data were calculated using SolX.<sup>55</sup>

**Fourier Transform Infrared (FT-IR) Spectroscopy.** IR spectra were recorded in attenuated reflectance mode using a Thermo Scientific Nicolet iS10 FT-IR spectrometer (Figure S4).

**Raman Vibration Spectroscopy.** Raman spectra were recorded on a Thermo Scientific DXR spectrometer (fine laser power: the control power was controlled and reported at samples in 0.1 mW increments) with a 760 nm laser source, between wavelengths of 100 and  $1200\text{ cm}^{-1}$  (Figure S4).

## RESULTS AND DISCUSSION

Discrete molecular cluster formation was achieved for each tetravalent metal by dissolving their corresponding salts;  $\text{Th}(\text{NO}_3)_4$ ,  $\text{U}(\text{SO}_4)_2$ , and  $\text{Ce}(\text{SO}_4)_2$  in 500–1000  $\mu\text{L}$  of water. Ammonium was added as a solution of  $(\text{NH}_4)_2\text{SO}_4$  in different concentrations for each metal. Crystal formation occurred during a mild hydrothermal treatment; see the SI for details. SCXRD on the products revealed that, for each tetravalent metal,  $\text{Th}^{\text{IV}}$ ,  $\text{U}^{\text{IV}}$ , and  $\text{Ce}^{\text{IV}}$ , a polyphasic crystalline material was obtained. Each crystalline phase was identified by both SCXRD and PXRD. Each crystal structure is described below. In summary, the crystalline phases range in size from highly coordinated monomers to complex supramolecular assemblies. Favored assemblies across the series are differentiated by  $\text{Th}^{\text{IV}}$ ,  $\text{U}^{\text{IV}}$ , and  $\text{Ce}^{\text{IV}}$  size and acidity (see Figure 1 for  $\text{Th}^{\text{IV}}$  and  $\text{U}^{\text{IV}}$  and Figures S1–S3 for  $\text{Ce}^{\text{IV}}$ ). Even with the isolation of common structures, such as the hexamer  $[\text{M}_6(\text{OH})_4(\text{O})_4]^{12+}$ , bonding and coordination differences lead to different arrangements for the capping sulfates and clusters within the lattice.

**Hexamer Formation with Ammonium.** The well-known hexamer core,  $[\text{An}_6(\text{OH})_4(\text{O})_4]^{12+}$ , is further ligated with sulfate and water molecules in different arrangements for  $\text{Th}^{\text{IV}}$ ,  $\text{U}^{\text{IV}}$ , and  $\text{Ce}^{\text{IV}}$ . For each of the four structures described below,

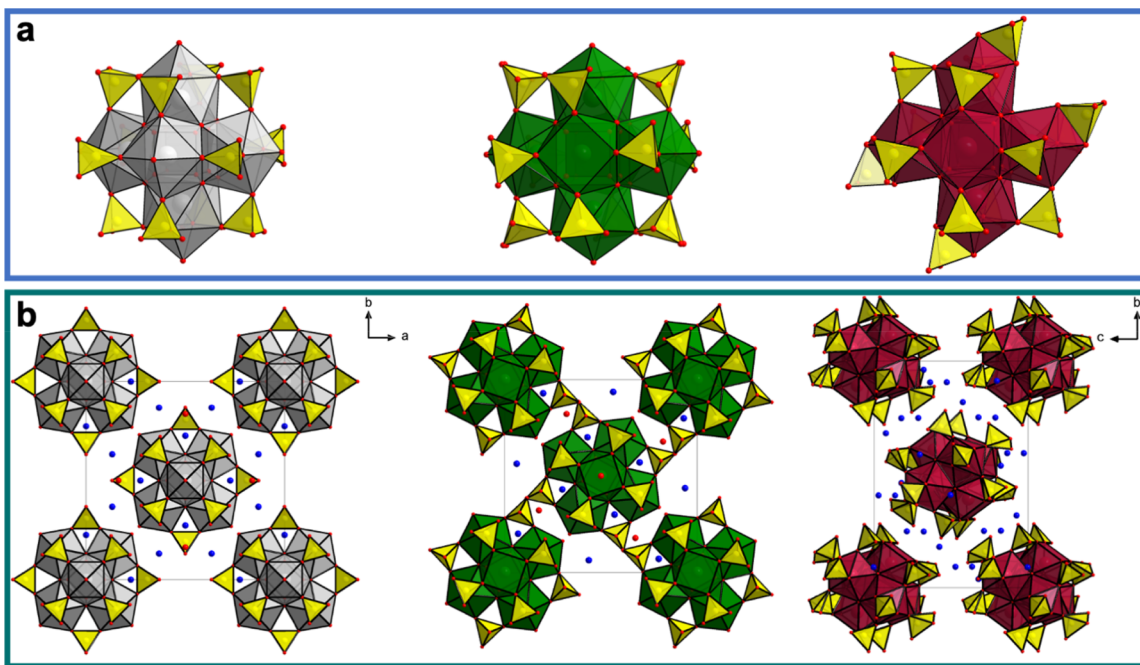


**Figure 3.** (a, left to right) Polyhedral representations of Th<sub>6</sub>, U<sub>6</sub>, and Ce<sub>6</sub>, showcasing the different orientations of capping sulfates and coordinating water molecules. (b, left to right) Lattice views of the hexamers for NH<sub>4</sub>Th<sub>6</sub>-tetra (NH<sub>4</sub>Th<sub>6</sub>-mono is shown in Figure S1) and NH<sub>4</sub>U<sub>6</sub> with tetragonal lattice symmetry, NH<sub>4</sub>Ce<sub>6</sub> (shown), and NH<sub>4</sub>Th<sub>6</sub>-mono (Figure S2A) crystallizing in monoclinic space groups. Th polyhedra are light gray, U polyhedra are green, Ce polyhedra are maroon, sulfates are yellow, O atoms are red spheres, and N atoms of the ammonium ions are blue spheres.

the four O<sup>2-</sup> and four OH<sup>-</sup> exhibit the typical complete disorder of 50% occupancy at each of the eight core sites. The M<sup>IV</sup>-O bond lengths are 2.180(2)-2.350(5) Å (Ce<sup>IV</sup>), 2.130(3)-2.344(9) Å (U<sup>IV</sup>), and 2.260(2)-2.3766(5) Å (Th<sup>IV</sup>). The M<sup>IV</sup>-OH bond lengths are 2.378(2)-2.572(10) Å (Ce<sup>IV</sup> and U<sup>IV</sup>) and 2.400(2)-2.560(6) Å (Th<sup>IV</sup>). The M<sup>IV</sup>-M<sup>IV</sup> distances are 3.779(15)-3.845(16) Å (Ce<sup>IV</sup>), 3.789(10)-3.921(15) Å (U<sup>IV</sup>), and 3.919(13)-4.096(13) Å (Th<sup>IV</sup>). This is what we expect based on their respective ionic radii, shorter bond lengths for smaller ionic radii.

Two NH<sub>4</sub>-Th<sub>6</sub> phases were isolated: NH<sub>4</sub>Th<sub>6</sub>-tetra (short for NH<sub>4</sub>Th<sub>6</sub>-tetragonal, abbreviations used herein), formulated as (NH<sub>4</sub>)<sub>12</sub>Th<sub>6</sub>(OH)<sub>4</sub>(O)<sub>4</sub>(SO<sub>4</sub>)<sub>12</sub>(H<sub>2</sub>O)<sub>6</sub>, crystallizes in the tetragonal space group I4/mmm [V = 3407.84(5) Å<sup>3</sup>] and NH<sub>4</sub>Th<sub>6</sub>-mono [also formulated as (NH<sub>4</sub>)<sub>12</sub>Th<sub>6</sub>(OH)<sub>4</sub>(O)<sub>4</sub>(SO<sub>4</sub>)<sub>12</sub>(H<sub>2</sub>O)<sub>6</sub>] crystallizes in monoclinic P2<sub>1</sub>/n [V = 3361.0(5) Å<sup>3</sup>; Table S2]. Both phases feature the [Th<sub>6</sub>(OH)<sub>4</sub>(O)<sub>4</sub>(SO<sub>4</sub>)<sub>12</sub>(H<sub>2</sub>O)<sub>6</sub>]<sup>12-</sup> cluster, the hexamer core with 12 capping sulfates, and six water molecules, resulting in 9-coordinate Th<sup>IV</sup> centers (Figure 3a, left). The 12 sulfates can be described as sitting on the edges of a cube, while the six polyhedra sit on the faces of the cube. The different crystal systems in which Th<sub>6</sub> is crystallized represents two different packing arrangements. Th-hexamers sit on the corners and center of the unit cell (Figure S5a shows NH<sub>4</sub>Th<sub>6</sub>-mono). For both cells, the Th<sub>6</sub> and ammonium cations are mainly associated by S-O---H-N hydrogen-bonding interactions at 2.5(4)-2.8(11) Å. In both structures, Th exhibits maximum coordination, consistent with it having the largest radii for tetravalent metals.

NH<sub>4</sub>-U<sub>6</sub>, formulated as (NH<sub>4</sub>)<sub>12</sub>U<sub>6</sub>(OH)<sub>4</sub>(O)<sub>4</sub>(SO<sub>4</sub>)<sub>12</sub>(H<sub>2</sub>O)<sub>4</sub>, crystallizes in the tetragonal space group P4/mnc [V = 3099.13(3) Å<sup>3</sup>; Table S3 and Figure 3b, center]. The 12-sulfate-capped hexamer,

[U<sub>6</sub>(OH)<sub>4</sub>(O)<sub>4</sub>(SO<sub>4</sub>)<sub>12</sub>(H<sub>2</sub>O)<sub>4</sub>]<sup>12-</sup>, has four water ligands, resulting in mixed U<sup>IV</sup> coordination (two 8-coordinate in a relative square-antiprismatic arrangement and four 9-coordinate in a capped square-antiprismatic arrangement; Figure 3a, left). The packing of U<sub>6</sub> accommodates the loss of two capping water molecules in a smaller cell compared to that of NH<sub>4</sub>Th<sub>6</sub>-tetra. There are contractions along the *a* and *b* axes by ~1 Å, which account for the loss in symmetry from face-centered (Th<sub>6</sub>) to primitive (U<sub>6</sub>). The loss of two capping water molecules results in the small contraction along the *c* axis (~0.5 Å). The smaller distance between the hexamers does not allow for two hexamers to have individual capping water molecules; an individual shared solvent water molecule 3.672(2) Å away (Figure S5b). Like the Th<sub>6</sub> structures, the ammonium cations are likewise associated by S-O---H-N hydrogen-bonding interactions at 2.5(5)-2.8(7) Å. The shorter bond lengths for U<sup>IV</sup> (compared to Th as discussed above) and the formation of 8-coordinate uranium are consistent with the comparatively smaller radii.

NH<sub>4</sub>Ce<sub>6</sub> features the first isolated Ce<sub>6</sub>-sulfate cluster. NH<sub>4</sub>Ce<sub>6</sub> is formulated as (NH<sub>4</sub>)<sub>16</sub>Ce<sub>6</sub>(OH)<sub>4</sub>(O)<sub>4</sub>(SO<sub>4</sub>)<sub>14</sub> and crystallizes in the monoclinic space group P2<sub>1</sub>/c [V = 3917(3) Å<sup>3</sup>; Table S4]. In [Ce<sub>6</sub>(OH)<sub>4</sub>(O)<sub>4</sub>(SO<sub>4</sub>)<sub>14</sub>]<sup>16-</sup>, two of the Ce<sup>IV</sup> centers, arranged in a relative trans position, have four sulfates that bridge to neighboring Ce polyhedra, similar to the arrangement of Th<sub>6</sub> and U<sub>6</sub>. The remaining four Ce centers are bridged via sulfates to three other Ce polyhedra and one sulfate that chelates the center in the capping position (where water resides in the Th<sub>6</sub> structure and partially in U<sub>6</sub>), and these Ce<sup>IV</sup> are 9-coordinate (Figure 3a, right). The lower symmetry and higher charge of this structure likely challenge its ordering into a lattice, and we hypothesize that this is why it has not been crystallized previously. Unlike Th<sub>6</sub> and U<sub>6</sub>, Ce<sub>6</sub> has no capping water molecules. It is interesting to note that the one with the

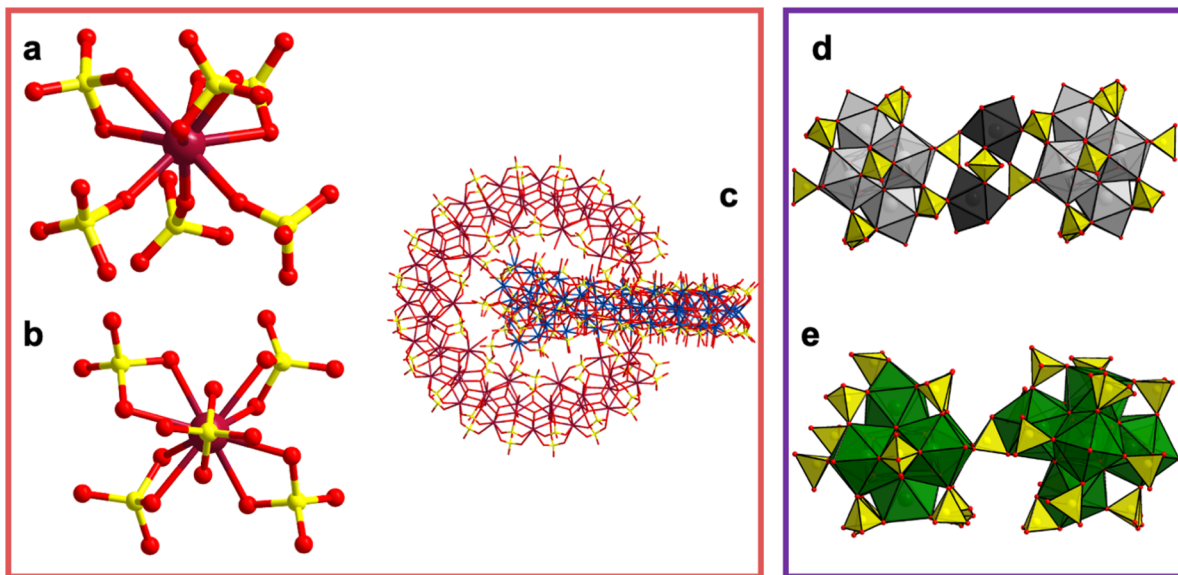


**Figure 4.** Ball-and-stick representation of (a)  $[\text{Ce}(\text{SO}_4)_6]^{8-}$ , showing three monodentate sulfates and three chelating sulfates. (b)  $[\text{Ce}(\text{SO}_4)_6]^{8-}$  showing all sulfates as chelating. (c) Wireframe representation of the Ce<sub>62</sub> dimer. Polyhedral representations of (d) NH<sub>4</sub>Th-Th<sub>6</sub> chains with Th monomers shown in black and (e) a NH<sub>4</sub>-U<sub>6</sub>-chain structure showing the linking sulfate. Th is light gray and black, U is green, sulfate is yellow, Ce is maroon and blue, and O is red.

smallest radius of M<sup>IV</sup> (Ce) has the same number of bonds in the hexamers as the one with biggest radius of M<sup>IV</sup> (Th), yet Ce favors sulfate over water. Perhaps bound water readily deprotonates, which challenges stabilization in a crystalline lattice. All Ce ions are tetravalent, according to bond-valence-sum (BVS) calculations (Table S5). The Ce<sub>6</sub> clusters are located in the center of the unit cell and on the four edges along the crystallographic *a* axis. In the extended lattice, they organize into layers on the *bc* plane, as opposed to pseudo-closest packing of the hexamers in the other described cells. This lower-symmetry organization can also be attributed to the lower-symmetry clusters. Once again, the ammonium ions appear to be associated by hydrogen bonding to the sulfates but at slightly longer distances [2.8(10)–3.0(15) Å].

We considered electrochemical studies on NH<sub>4</sub>-Ce<sub>6</sub>, but prior studies by Antonio suggest that these experiments would be unfruitful.<sup>56</sup> All of the M<sup>IV</sup><sub>6</sub> hexamers carry a negative charge because of the strongly bound sulfate ligands; for example, NH<sub>4</sub>-Ce<sub>6</sub> carries a 16<sup>-</sup> charge. This is in contrast to Antonio's Ce hexamer with an 8+ charge (formulated as  $[\text{Ce}_6(\mu_3\text{-O})_4(\mu_3\text{-OH})_4(\text{NH}_3\text{CH}_2\text{COO})_8(\text{NO}_3)_4(\text{H}_2\text{O})_6]\text{Cl}_8 \cdot 8\text{H}_2\text{O}$ ).<sup>56</sup> For this previously reported Ce<sub>6</sub> cluster, cyclic voltammetry (CV) found a large negative shift for the Ce<sup>IV/III</sup> couple compared to the monomer. Therefore, we suspect that the tetravalent oxidation state is stabilized in the polynuclear form. Moreover, Antonio's CV was irreversible because the hexamer dissociates upon reduction. In addition, we found that any Ce<sup>III</sup> in our previously reported Ce<sub>70</sub> rings existed in the structure as a monomer form.<sup>25</sup>

**Phases beyond the Hexamer: Monomers to Supramolecular Assembly.** From this point forward, we further differentiate the chemistries between Th<sup>IV</sup>, U<sup>IV</sup>, and Ce<sup>IV</sup> in five additional structures. Differences in the size and acidity dictate the more complex and diverging structural behavior, beyond the isolated hexamers. Discussed below are additional phases that cocrystallize with the hexamer phases described above (Figure 2a,b).

Additional Ce<sup>IV</sup> structures include two cerium sulfate monomer units and the Ce<sub>62</sub> phase. A previous study showed that different concentrations of ammonium during cluster formation yielded the isolation of different cluster fragments.<sup>25</sup> This study further demonstrates that Ce species in the ammonium sulfate system range from monomers to Ce<sub>62</sub> that coexist both in solution (seen in the next section) and in the solid state. The monomers (NH<sub>4</sub>)<sub>6</sub>Ce(SO<sub>4</sub>)<sub>5</sub> and (NH<sub>4</sub>)<sub>8</sub>Ce(SO<sub>4</sub>)<sub>6</sub> respectively crystallize in the monoclinic space group P<sub>2</sub><sub>1</sub>/m [ $V = 2496.00(7)$  Å<sup>3</sup>] and in the trigonal space group P3 [ $V = 1464.07(3)$  Å<sup>3</sup>; Table S4 and Figure 4a,b]. These species represent high coordination environments (9- and 10-coordinate BVS respectively in Tables S5 and S6) not typically seen for Ce<sup>IV</sup> but consistent with the size and acidity of Ce<sup>IV</sup>. These two structures, as previously mentioned, cocrystallize with Ce<sub>6</sub> and Ce<sub>62</sub> (as described below). However, their significance as cocrystallites becomes more apparent when the crystal data are complemented with solution characterization later. NH<sub>4</sub>-(Ce<sub>62</sub>)<sub>2</sub>-mono is formulated as (NH<sub>4</sub>)<sub>82</sub>(Ce<sub>62</sub>(OH)<sub>30</sub>(O)<sub>58</sub>(SO<sub>4</sub>)<sub>71</sub>(H<sub>2</sub>O)<sub>33.25</sub>)(Ce<sub>62</sub>(OH)<sub>30</sub>(O)<sub>58</sub>(SO<sub>4</sub>)<sub>72</sub>(H<sub>2</sub>O)<sub>36.5</sub>) and crystallizes in the monoclinic space group P2<sub>1</sub>/n [ $V = 120929.6(12)$  Å<sup>3</sup>; Table S4]. We previously reported the Ce<sub>62</sub> structure in 2021 (in a triclinic P1 cell), but it is described here again briefly for convenience. This structure can best be described when first considering Ce<sub>70</sub>, [Ce<sub>70</sub>(OH)<sub>36</sub>(O)<sub>64</sub>(SO<sub>4</sub>)<sub>60</sub>]<sup>4-</sup>. Ce<sub>70</sub> is composed of 10 Ce<sub>6</sub> and 10 Ce<sub>monomers</sub>, bridged by sulfates into a toroid shape. Ce<sub>62</sub> is an incomplete fragment of Ce<sub>70</sub>, missing a Ce<sub>6</sub> and two Ce<sub>monomers</sub>. The Ce<sub>62</sub> fragment is thus stabilized by forming a dimer and mediating interactions through the ammonium ions. Further addenda sulfates decorate the ring and also interact with the ammoniums. Ammonium is the only known cation to promote and stabilize the Ce<sub>62</sub> dimer (Figure 4c,d). Isolation of the monoclinic phase for Ce<sub>62</sub> also shows slightly higher ordering behavior, like the superatom behavior of U<sub>84</sub>, by crystallizing in a higher symmetry lattice. The multiple phases show that manipulation of the lattice formation can be extended to Ce<sub>62</sub>, akin to the

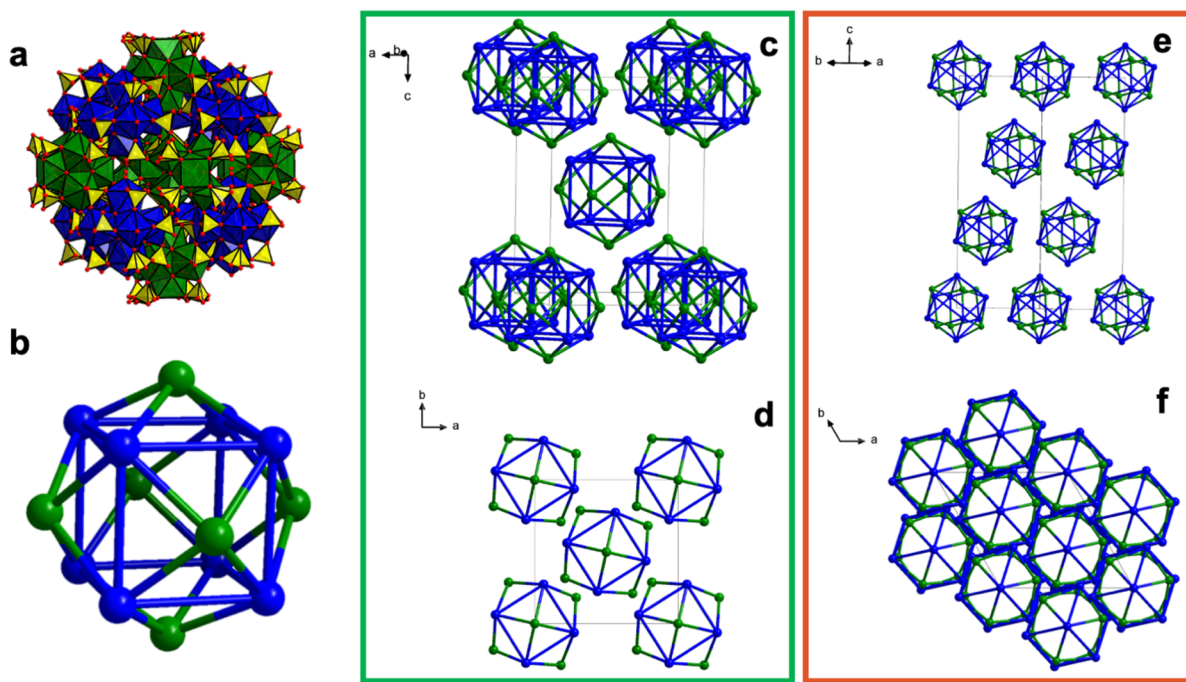


**Figure 5.** Polyhedral representation of (a)  $\text{U}_{84}$  with hexamers in the corner of the cube in blue and hexamers in the face of the cube in green. (b) Ball-and-stick representation, with hexamers as a single large sphere for ease of viewing. (c) View perpendicular to the  $c$  axis, with the leading hexamer on the face of the cube shown in green. (d) View parallel to the  $c$  axis showing tetragonal lattice symmetry. (e) View perpendicular to the  $c$  axis, with the leading hexamer on the corner of the cube shown in blue. (f) View parallel to the  $c$  axis showing trigonal lattice symmetry. U and  $\text{U}_6$  are shown in blue and green, S is shown in yellow, and O is shown in red. Modified with permission from ref 22. Copyright 2020 American Chemical Society.

previously shown postsynthesis addition of  $\text{Ce}^{\text{III}}$  monomers to the  $\text{Ce}_{62}$  dimer.<sup>25</sup>

Monomer formation was also observed for Th, albeit within the  $\text{NH}_4\text{Th}-\text{Th}_6$  lattice, linking  $\text{Th}_6$  into chains.  $\text{NH}_4\text{Th}-\text{Th}_6$  is formulated as  $(\text{NH}_4)_8(\text{Th}(\text{SO}_4)_4(\text{H}_2\text{O})_3)_2\text{Th}_6(\text{OH})_4(\text{O})_4(\text{SO}_4)_{12}(\text{H}_2\text{O})_5$  and crystallizes in the triclinic space group  $P\bar{1}$  [ $V = 2075.06(14)$  Å<sup>3</sup>; Table S2]. The  $[\text{Th}(\text{SO}_4)(\text{H}_2\text{O})_3]^{2+}$  monomers coordinate on opposite faces of the hexamers. Each Th monomer is bridged to an adjacent hexamer via three sulfates and to each other via two sulfates. This leads to chains along the  $c$  axis of alternating hexamer and two monomers; two hexamers joined by monomers are shown in Figures 4e and S3a. All Th<sup>IV</sup> are 9-coordinate, and the bond lengths are consistent with the  $\text{Th}_6$  structures above. Ammonium ions are located between the chains and associated by hydrogen bonding. The synthesis procedures reported in the SI represent the optimal conditions for crystal formation. However, multiple experiments, by the variation of parameters such as concentration, temperature and time of heating, and reagent ratios, did not reveal new or larger species than those reported here. Thus, we concluded that the lack of observable new species remains consistent with its lower acidity.

$\text{U}^{\text{IV}}$  also formed hexamer chains, but without participation of monomers.  $\text{NH}_4\text{-}\text{U}_6$  chains, formulated as  $(\text{NH}_4)_{12}\text{U}_6(\text{OH})_4(\text{O})_4(\text{SO}_4)_{12}(\text{H}_2\text{O})_5$ , crystallize in the triclinic space group  $P\bar{1}$  [ $V = 6159.0(5)$  Å<sup>3</sup>; Table S3 and Figure 4f]. The hexamers are bridged only by a single sulfate that also caps the hexamers, and the chains run “zigzag” approximately along the  $b$  axis (Figure S6b). Three of the six U centers have a capping water, creating a 9-coordinate  $\text{U}^{\text{IV}}$ . Two of the remaining three  $\text{U}^{\text{IV}}$  centers have chelating sulfates; however,

the long bond lengths of 2.87(2)–2.97(2) Å suggest an 8-coordinate environment instead. The bond lengths and coordination are consistent with the  $\text{NH}_4\text{U}_6$  structure (Table S8).

As aforementioned, PXRD reveals that the  $\text{U}_6$  chain phase always cocrystallizes with the isolated  $\text{U}_6$  counterpart (Figure 2a). However, a slight modification to the synthesis yields  $\text{U}_{84}$ , a more complex supramolecular assembly of  $\text{U}_6$ , but still bridged by sulfates that cap the hexamers. By doubling the concentration of the uranium(IV) sulfate solution (see the SI for details),  $\text{U}_{84}$  can be isolated with ammonium counterions. We first reported the  $\text{U}_{84}$  structure in 2020, isolated with lanthanide counterions and a 0.5 M sulfuric acid solution, used to solubilize  $\text{Ln}_2\text{O}_3$ . We concluded at the time that the acid prevented the formation of  $\text{U}_{70}$  (more extensive hydrolysis).<sup>22</sup> However, in this study, only  $(\text{NH}_4)_2\text{SO}_4$  was used as an electrolyte, without added acid. However, we might conclude for the current study that a higher concentration of  $\text{U}_6$  provides the opportunity for a second-order supramolecular assembly of  $\text{U}_{84}$  from  $\text{U}_6$  building units.

Briefly,  $\text{U}_{84}$  can be described as a cage of 14  $\text{U}_6$  (8 sit on the corner of a cube and 6 on the face of a cube), and they are linked by bridging sulfates (Figure 5a,b; formulated as  $[(\text{U}_6(\text{OH})_4(\text{O})_4)_{14}(\text{SO}_4)_{120}(\text{H}_2\text{O})_{42}]^{72-}$ ). With ammonium counterions,  $\text{U}_{84}$  is isolated as a discrete structure (meaning that they are not linked to each other via bridging cations, as was observed in prior structures) crystallizing in two different lattices.<sup>22</sup> Both phases, generally formulated as  $(\text{NH}_4)_{72}(\text{U}_6(\text{OH})_4(\text{O})_4)_{14}(\text{SO}_4)_{120}(\text{H}_2\text{O})_{42}$ , crystallized in the tetragonal space group  $I4/m$  [ $V = 35110.9(5)$  Å<sup>3</sup>] and in the trigonal space group  $R\bar{3}$  [ $V = 57471.3(6)$  Å<sup>3</sup>; Table S3 and Figure 5c–f]. The formation of these two lattices arises from

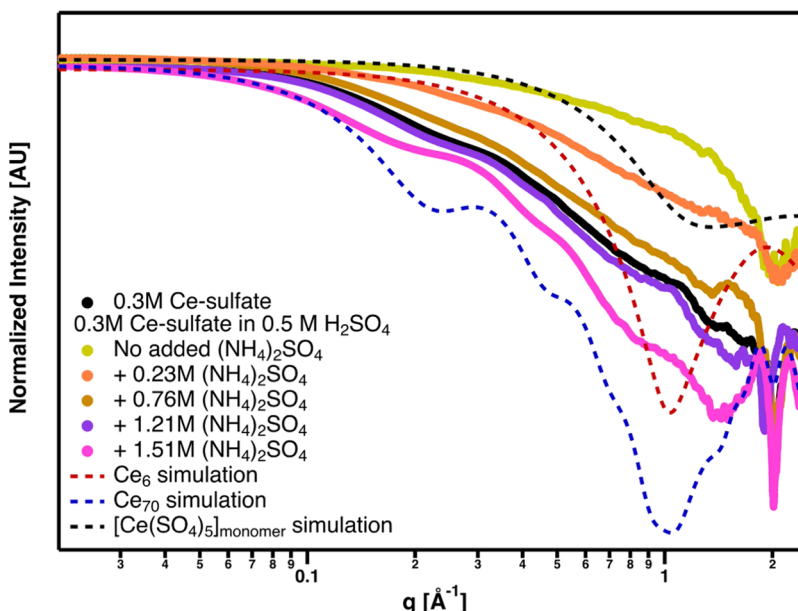


**Figure 6.** SAXS of a 0.3 M Ce(SO<sub>4</sub>)<sub>2</sub> solution in 0.5 M H<sub>2</sub>SO<sub>4</sub> and with increasing addition of (NH<sub>4</sub>)<sub>2</sub>SO<sub>4</sub>.

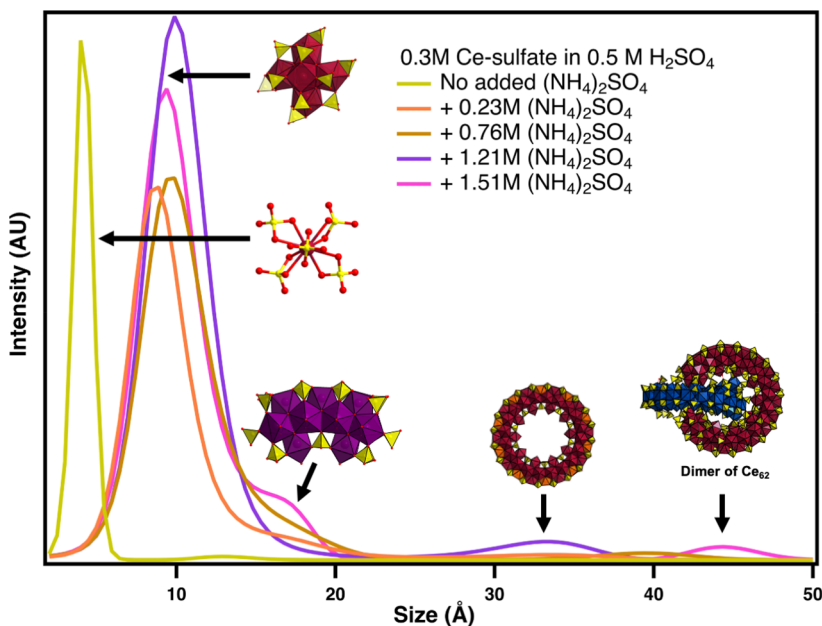


**Figure 7.** Size distribution analysis showing the growth from monomers to hexamers to fully formed rings and the Ce<sub>62</sub> dimer.

the symmetry and stacking of U<sub>84</sub>. Considering the symmetry of U<sub>84</sub> as a cube, there can be a 3- or 4-fold symmetry when stacking along the corner or face of the cube, respectively. As such, when U<sub>84</sub> assembles into a lattice, two orientations are possible along the *c* axis. If the leading hexamer along the *c* axis is on the “face” of U<sub>84</sub>, then a 4-fold symmetry is made perpendicular to the axis, resulting in a tetragonal lattice symmetry (Figure 5c,d). If the leading hexamer along the *c* axis is on the “corner” of U<sub>84</sub>, then a 3-fold symmetry is made perpendicular to the axis, resulting in a trigonal lattice symmetry (Figure 5e,f). As with Th<sup>IV</sup> and Ce<sup>IV</sup>, no other crystalline phases could be identified by SCXRD or PXRD, and the lack of any further oligomerization into larger metal–oxo species was not observed.

**Tracking Assemblies in Solution.** We used SAXS to track the formation of Th<sup>IV</sup>, U<sup>IV</sup>, or Ce<sup>IV</sup> clusters as a function

of the ammonium concentration. This provides a snapshot of the solution processes that lead to the structures described above. Attempts to mimic the synthesis conditions could only be extended to the parameter of counterion concentration because other parameters are crucial in the formation of some species; such as heating, becomes untenable because of either the current system setup or the rapid crystallization of species, which is our main issue. As such, the solution concentration for each metal was constant at 0.3 M to maintain consistency with the synthetic conditions that have led to crystal growth. In the case for Ce<sup>IV</sup>, a previous study showed that, even at high acidity and high concentration, dissolved Ce(SO<sub>4</sub>)<sub>2</sub> shows a high degree of polymerization.<sup>25</sup> Herein we show that ammonium counterions have an effect similar to that of Li<sup>+</sup> (shown previously) in promoting cluster formation (Figure 6). The Ce<sup>IV</sup> solution was modified to 0.3 M cerium sulfate in 0.5

M H<sub>2</sub>SO<sub>4</sub> to minimize the inherent high degree of polymerization (black scattering curve in Figure 6a), as seen by the downward slope starting at  $q = 0.1 \text{ \AA}^{-1}$ . The higher acidity and sulfate system for Ce<sup>IV</sup> allowed us to differentiate cluster formation more clearly by the cation versus inherent oligomerization. In this solution, [Ce(SO<sub>4</sub>)<sub>x</sub>]<sup>4-2x</sup> not only could be identified but also was shown to be the predominant species and starting point in cation-induced cluster formation (Figure 7).

The addition of ammonium as (NH<sub>4</sub>)<sub>2</sub>SO<sub>4</sub> shifts the Guinier region (the elbow where the scattering intensity descends) to lower  $q$ . In addition, distinctive features indicative of the Ce<sub>70</sub> shape and size are seen by the pair of peaks at high  $q$  (1.9 and 2.1  $\text{\AA}^{-1}$ ) and by the growth of an oscillation around  $q = 0.3 \text{ \AA}^{-1}$ . Size distribution analyses were performed on the SAXS curves to estimate species size and track their evolution with increasing NH<sub>4</sub><sup>+</sup>. The data are summarized in Table S10, and scattering curve fits are shown in Figure S8. The size distribution analysis of simple Ce(SO<sub>4</sub>)<sub>2</sub> in a 0.5 M H<sub>2</sub>SO<sub>4</sub> solution suggests that >97% of the dissolved species are highly coordinated Ce monomers, [Ce(SO<sub>4</sub>)<sub>5/6</sub>]<sup>6-/8-</sup>. At 0.23, 0.76, 1.12, and 1.51 M (NH<sub>4</sub>)<sub>2</sub>SO<sub>4</sub>, the predominate species (>80%) is Ce<sub>6</sub>, as described above (Figure 7). The poor solubility of Ce<sub>70</sub> contributes to the low percent population [approximately 5.8% at 1.21 M (NH<sub>4</sub>)<sub>2</sub>SO<sub>4</sub>], even at high ammonium concentration. At 1.51 M (NH<sub>4</sub>)<sub>2</sub>SO<sub>4</sub>, the largest species has a diameter of 44  $\text{\AA}$ , which corresponds to the size of the Ce<sub>62</sub> dimer (Figure S9). Intermediate-size species (~16  $\text{\AA}$  in diameter) were also detected and attributed to the Ce<sub>13</sub> fragment. Parallel studies with U<sup>IV</sup> and Th<sup>IV</sup> also showed a trend of increasing size with the addition of NH<sub>4</sub><sup>+</sup> (Figure S10). However, the size species in solution only became slightly larger than that of a monomer, perhaps simply because of increasing ligation with sulfate (replacing hydration spheres). There is also an increase in the polydispersity (noted by the shallowing of the slope), and this is likely due to a varying amount of sulfate coordination and even dimer formation. It is only after a mild hydrothermal treatment that we can see larger species such as U<sub>84</sub> (Figure S11).

## CONCLUSION

The tetravalent metals Ce<sup>IV</sup>, Th<sup>IV</sup>, U<sup>IV</sup>, Np<sup>IV</sup>, and Pu<sup>IV</sup> with their common oxidation states provide the opportunity to understand hydrolysis trends of similar metal cations across the periodic table. Here, using sulfate as a capping group and ammonium for rapid crystallization, we described by SCXRD the formation of the common hexamers for Th<sup>IV</sup>, U<sup>IV</sup>, and Ce<sup>IV</sup>, showcasing some of the similarities and differences in their chemistry. While relatively “soft” Th<sup>IV</sup> produced only hexamer- and monomer-linked hexamer chains, U<sup>IV</sup> and Ce<sup>IV</sup> yielded supramolecular assemblies of hexamers, U<sub>84</sub>, and the Ce<sub>62</sub> dimer. Room temperature solution-phase studies (SAXS) broadly showed, for all three M<sup>IV</sup>, that sulfuric acid suppressed oligomerization, and polynuclear clusters did not form. While ammonium sulfate had little effect on Th<sup>IV</sup> and U<sup>IV</sup> cluster formation, it promoted rapid cluster assembly for Ce<sup>IV</sup>, highlighting a distinctly different behavior. From the prospective of a periodic trend, we indeed expect more extensive polymerization with decreasing metal-cation size (Th<sup>IV</sup> > U<sup>IV</sup> > Ce<sup>IV</sup>), commensurate with increased acidity, in other words, looking at the hydrolysis and condensation behavior for transuranic elements such as Pu<sup>IV</sup> and Np<sup>IV</sup>. However, the difference between Ce<sup>IV</sup> and Th/U<sup>IV</sup> (room

temperature solution phase) is very stark, suggesting that something else is at play, i.e., the facile redox behavior, which will be investigated in future studies.

## ASSOCIATED CONTENT

### Supporting Information

The Supporting Information is available free of charge at <https://pubs.acs.org/doi/10.1021/acs.inorgchem.2c01309>.

Experimental details, PXRD patterns, IR and Raman spectra, crystallographic information on the 11 structures, BVS on Ce structures, bond-length and solvent-void-mask summaries, and SAXS curves of NH<sub>4</sub><sup>+</sup> addition for U and Th (PDF)

## Accession Codes

CCDC 2105625–2105632, 2105637, 2164765, and 2164766 contain the supplementary crystallographic data for this paper. These data can be obtained free of charge via [www.ccdc.cam.ac.uk/data\\_request/cif](http://www.ccdc.cam.ac.uk/data_request/cif), or by emailing [data\\_request@ccdc.cam.ac.uk](mailto:data_request@ccdc.cam.ac.uk), or by contacting The Cambridge Crystallographic Data Centre, 12 Union Road, Cambridge CB2 1EZ, UK; fax: +44 1223 336033.

## AUTHOR INFORMATION

### Corresponding Authors

Ian Colliard — Department of Chemistry, Oregon State University, Corvallis, Oregon 97331, United States;  
ORCID: [0000-0003-1883-1155](https://orcid.org/0000-0003-1883-1155); Email: [colliari@oregonstate.edu](mailto:colliari@oregonstate.edu)

May Nyman — Department of Chemistry, Oregon State University, Corvallis, Oregon 97331, United States; Email: [may.nyman@oregonstate.edu](mailto:may.nyman@oregonstate.edu)

### Author

Jessica C. Brown — Department of Chemistry, Oregon State University, Corvallis, Oregon 97331, United States

Complete contact information is available at: <https://pubs.acs.org/10.1021/acs.inorgchem.2c01309>

## Notes

The authors declare no competing financial interest.

## ACKNOWLEDGMENTS

This study was supported by the Department of Energy, National Nuclear Security Administration under Award DE-NA0003763. We acknowledge the Murdock Charitable Trust (Grant SR-2017297) for acquisition of the single-crystal X-ray diffractometer.

## REFERENCES

- (1) Moons, J.; Azambuja, F.; Mihailovic, J.; Kozma, K.; Smiljanic, K.; Amiri, M.; Cirkovic Velickovic, T.; Nyman, M.; Parac-Vogt, T. N. Discrete Hf 18 Metal-oxo Cluster as a Heterogeneous Nanozyme for Site-Specific Proteolysis. *Angew. Chem., Int. Ed.* **2020**, 59 (23), 9094–9101.
- (2) Benedetti, C.; Cazzolaro, A.; Carraro, M.; Graf, R.; Landfester, K.; Gross, S.; Muñoz-Espí, R. Dual Role of Zirconium Oxoclusters in Hybrid Nanoparticles: Cross-Linkers and Catalytic Sites. *ACS Appl. Mater. Interfaces* **2016**, 8 (39), 26275–26284.
- (3) Wang, X.; Brunson, K.; Xie, H.; Colliard, I.; Wasson, M. C.; Gong, X.; Ma, K.; Wu, Y.; Son, F. A.; Idrees, K. B.; Zhang, X.; Notestein, J. M.; Nyman, M.; Farha, O. K. Heterometallic Ce<sup>IV</sup>/VV Oxo Clusters with Adjustable Catalytic Reactivities. *J. Am. Chem. Soc.* **2021**, 143 (49), 21056–21065.

- (4) Jakobsen, S.; Gianolio, D.; Wragg, D. S.; Nilsen, M. H.; Emerich, H.; Bordiga, S.; Lamberti, C.; Olsbye, U.; Tilset, M.; Lillerud, K. P. Structural determination of a highly stable metal-organic framework with possible application to interim radioactive waste scavenging: Hf–UiO-66. *Phys. Rev. B* **2012**, *86* (12), 125429.
- (5) Dhall, A.; Self, W. Cerium Oxide Nanoparticles: A Brief Review of Their Synthesis Methods and Biomedical Applications. *Antioxidants* **2018**, *7* (8), 97.
- (6) Wilson, R. E.; Skanthakumar, S.; Soderholm, L. Separation of Plutonium Oxide Nanoparticles and Colloids. *Angew. Chem., Int. Ed.* **2011**, *50* (47), 11234–11237.
- (7) Sigmon, G. E.; Hixon, A. E. Extension of the Plutonium Oxide Nanocluster Family to Include {Pu 16} and {Pu 22}. *Chem. Eur. J.* **2019**, *25* (10), 2463–2466.
- (8) Martin, N. P.; März, J.; Feuchter, H.; Duval, S.; Roussel, P.; Henry, N.; Ikeda-Ohno, A.; Loiseau, T.; Volkrieger, C. Synthesis and structural characterization of the first neptunium based metal–organic frameworks incorporating {Np<sub>6</sub>O<sub>8</sub>} hexanuclear clusters. *Chem. Commun.* **2018**, *54* (51), 6979–6982.
- (9) Lammert, M.; Wharmby, M. T.; Smolders, S.; Bueken, B.; Lieb, A.; Lomachenko, K. A.; Vos, D. D.; Stock, N. Cerium-based metal organic frameworks with UiO-66 architecture: synthesis, properties and redox catalytic activity. *Chem. Commun.* **2015**, *51* (63), 12578–12581.
- (10) Falaise, C.; Volkrieger, C.; Vigier, J.-F.; Henry, N.; Beaurain, A.; Loiseau, T. Three-Dimensional MOF-Type Architectures with Tetravalent Uranium Hexanuclear Motifs (U<sub>6</sub>O<sub>8</sub>). *Chem. Eur. J.* **2013**, *19* (17), 5324–5331.
- (11) Falaise, C.; Charles, J.-S.; Volkrieger, C.; Loiseau, T. Thorium Terephthalates Coordination Polymers Synthesized in Solvothermal DMF/H<sub>2</sub>O System. *Inorg. Chem.* **2015**, *54* (5), 2235–2242.
- (12) Hastings, A. M.; Ray, D.; Jeong, W.; Gagliardi, L.; Farha, O. K.; Hixon, A. E. Advancement of Actinide Metal–Organic Framework Chemistry via Synthesis of Pu–UiO-66. *J. Am. Chem. Soc.* **2020**, *142* (20), 9363–9371.
- (13) Henry, M.; Jolivet, J. P.; Livage, J. Aqueous chemistry of metal cations: Hydrolysis, condensation and complexation. In *Chemistry, Spectroscopy and Applications of Sol–Gel Glasses*; Reisfeld, R., Jørgensen, C. K., Eds.; Springer: Berlin, 1992; pp 153–206.
- (14) Sommers, J. A.; Hutchison, D. C.; Martin, N. P.; Palys, L.; Amador, J. M.; Keszler, D. A.; Nyman, M. Differentiating Zr/HfIV Aqueous Polyoxocation Chemistry with Peroxide Ligation. *Inorg. Chem.* **2021**, *60* (3), 1631–1640.
- (15) Sommers, J. A.; Palys, L.; Martin, N. P.; Fast, D. B.; Amiri, M.; Nyman, M. Oxo-Cluster-Based Zr/HfIV Separation: Shedding Light on a 70-Year-Old Process. *J. Am. Chem. Soc.* **2022**, *144* (6), 2816–2824.
- (16) Sommers, J. A.; Hutchison, D. C.; Martin, N. P.; Kozma, K.; Keszler, D. A.; Nyman, M. Peroxide-Promoted Disassembly Reassembly of Zr-Polyoxocations. *J. Am. Chem. Soc.* **2019**, *141* (42), 16894–16902.
- (17) Oleksak, R. P.; Ruther, R. E.; Luo, F.; Amador, J. M.; Decker, S. R.; Jackson, M. N.; Motley, J. R.; Stowers, J. K.; Johnson, D. W.; Garfunkel, E. L.; Keszler, D. A.; Herman, G. S. Evaluation of Thermal and Radiation Induced Chemistries of Metal Oxo–Hydroxo Clusters for Next-Generation Nanoscale Inorganic Resists. *ACS Appl. Nano Mater.* **2018**, *1* (9), 4548–4556.
- (18) Hennig, C.; Weiss, S.; Kraus, W.; Kretschmar, J.; Scheinost, A. C. Solution Species and Crystal Structure of Zr(IV) Acetate. *Inorg. Chem.* **2017**, *56* (5), 2473–2480.
- (19) Takao, S.; Takao, K.; Kraus, W.; Emmerling, F.; Scheinost, A. C.; Bernhard, G.; Hennig, C. First Hexanuclear UIVand ThIVFormate Complexes - Structure and Stability Range in Aqueous Solution. *Eur. J. Inorg. Chem.* **2009**, *2009* (32), 4771–4775.
- (20) Knope, K. E.; Soderholm, L. Plutonium(IV) Cluster with a Hexanuclear [Pu<sub>6</sub>(OH)<sub>4</sub>O<sub>4</sub>]<sup>12+</sup> Core. *Inorg. Chem.* **2013**, *52* (12), 6770–6772.
- (21) Knope, K. E.; Vasiliu, M.; Dixon, D. A.; Soderholm, L. Thorium(IV)–Selenate Clusters Containing an Octanuclear Th(IV) Hydroxide/Oxide Core. *Inorg. Chem.* **2012**, *51* (7), 4239–4249.
- (22) Colliard, I.; Morrison, G.; Loye, H.-C. Z.; Nyman, M. Supramolecular Assembly of U(IV) Clusters and Superatoms with Unconventional Counterions. *J. Am. Chem. Soc.* **2020**, *142* (19), 9039–9047.
- (23) Colliard, I.; Nyman, M. Building [U IV 70 (OH) 36 (O) 64] 4– Oxocluster Frameworks with Sulfate, Transition Metals, and U V. *Chem. Eur. J.* **2020**, *26* (54), 12481–12488.
- (24) Colliard, I.; Nyman, M. Ce<sup>IV</sup><sub>70</sub> oxosulfate rings, frameworks, supramolecular assembly and redox activity. *Angew. Chem., Int. Ed.* **2021**, *60*, 7308.
- (25) Colliard, I.; Brown, J. C.; Fast, D. B.; Sockwell, A. K.; Hixon, A. E.; Nyman, M. Snapshots of Ce<sub>70</sub> Toroid Assembly from Solids and Solution. *J. Am. Chem. Soc.* **2021**, *143* (25), 9612–9621.
- (26) Jin, G. B.; Lin, J.; Estes, S. L.; Skanthakumar, S.; Soderholm, L. Influence of Counterion Hydration Enthalpies on the Formation of Molecular Complexes: A Thorium–Nitrate Example. *J. Am. Chem. Soc.* **2017**, *139* (49), 18003–18008.
- (27) Dufaye, M.; Martin, N. P.; Duval, S.; Volkrieger, C.; Ikeda-Ohno, A.; Loiseau, T. Time-controlled synthesis of the 3D coordination polymer U(1,2,3-Hbtc)2 followed by the formation of molecular poly-oxo cluster {U14} containing hemimellitate uranium(iv). *RSC Adv.* **2019**, *9* (40), 22795–22804.
- (28) Nocton, G.; Pécaut, J.; Filinchuk, Y.; Mazzanti, M. Ligand assisted cleavage of uranium oxo-clusters. *Chem. Commun.* **2010**, *46* (16), 2757–2759.
- (29) Biswas, B.; Mougel, V.; Pécaut, J.; Mazzanti, M. Base-Driven Assembly of Large Uranium Oxo/Hydroxo Clusters. *Angew. Chem., Int. Ed.* **2011**, *50* (25), 5745–5748.
- (30) Mitchell, K. J.; Abboud, K. A.; Christou, G. Atomically-precise colloidal nanoparticles of cerium dioxide. *Nat. Commun.* **2017**, *8* (1). DOI: [10.1038/s41467-017-01672-4](https://doi.org/10.1038/s41467-017-01672-4)
- (31) Russell-Webster, B.; Lopez-Nieto, J.; Abboud, K. A.; Christou, G. Truly Monodisperse Molecular Nanoparticles of Cerium Dioxide of 2.4 nm dimensions: A {Ce 100 O 167} Cluster. *Angew. Chem., Int. Ed.* **2021**, *60* (22), 12591–12596.
- (32) Mitchell, K. J.; Goodsell, J. L.; Russell-Webster, B.; Twahir, U. T.; Angerhofer, A.; Abboud, K. A.; Christou, G. Expansion of the Family of Molecular Nanoparticles of Cerium Dioxide and Their Catalytic Scavenging of Hydroxyl Radicals. *Inorg. Chem.* **2021**, *60* (3), 1641–1653.
- (33) Wasson, M. C.; Zhang, X.; Otake, K.-I.; Rosen, A. S.; Alayoglu, S.; Krzyaniak, M. D.; Chen, Z.; Redfern, L. R.; Robison, L.; Son, F. A.; Chen, Y.; Islamoglu, T.; Notestein, J. M.; Snurr, R. Q.; Wasieleski, M. R.; Farha, O. K. Supramolecular Porous Assemblies of Atomically Precise Catalytically Active Cerium-Based Clusters. *Chem. Mater.* **2020**, *32* (19), 8522–8529.
- (34) Soderholm, L.; Almond, P. M.; Skanthakumar, S.; Wilson, R. E.; Burns, P. C. The Structure of the Plutonium Oxide Nanocluster [Pu<sub>38</sub>O<sub>56</sub>Cl<sub>54</sub>(H<sub>2</sub>O)<sub>8</sub>]<sup>14-</sup>. *Angew. Chem., Int. Ed.* **2008**, *47* (2), 298–302.
- (35) Falaise, C.; Volkrieger, C.; Vigier, J.-F.; Beaurain, A.; Roussel, P.; Rabu, P.; Loiseau, T. Isolation of the Large {Actinide}38 Poly-oxo Cluster with Uranium. *J. Am. Chem. Soc.* **2013**, *135* (42), 15678–15681.
- (36) Martin, N. P.; Volkrieger, C.; Henry, N.; Trivelli, X.; Stoclet, G.; Ikeda-Ohno, A.; Loiseau, T. Formation of a new type of uranium(iv) poly-oxo cluster {U38} based on a controlled release of water via esterification reaction. *Chemical Science* **2018**, *9* (22), 5021–5032.
- (37) Vanagas, N. A.; Higgins, R. F.; Wacker, J. N.; Asuogui, D. R. C.; Warzecha, E.; Kozimor, S. A.; Stoll, S. L.; Schelter, E. J.; Bertke, J. A.; Knope, K. E. Mononuclear to Polynuclear U IV Structural Units: Effects of Reaction Conditions on U-Furoate Phase Formation. *Chem. Eur. J.* **2020**, *26* (26), 5872–5886.
- (38) Martin, N. P.; Volkrieger, C.; Roussel, P.; März, J.; Hennig, C.; Loiseau, T.; Ikeda-Ohno, A. {Np38} clusters: the missing link in the

largest poly-oxo cluster series of tetravalent actinides. *Chem. Commun.* **2018**, *54* (72), 10060–10063.

(39) Falaise, C.; Kozma, K.; Nyman, M. Thorium Oxo-Clusters as Building Blocks for Open Frameworks. *Chem. Eur. J.* **2018**, *24* (53), 14226–14232.

(40) Lin, J.; Jin, G. B.; Soderholm, L. Th<sub>3</sub>[Th<sub>6</sub>(OH)<sub>4</sub>O<sub>4</sub>(H<sub>2</sub>O)<sub>6</sub>](SO<sub>4</sub>)<sub>12</sub>(H<sub>2</sub>O)<sub>13</sub>: A Self-Assembled Microporous Open-Framework Thorium Sulfate. *Inorg. Chem.* **2016**, *55* (20), 10098–10101.

(41) Woidy, P.; Kraus, F. [Th<sub>10</sub>(μ-F<sub>16</sub>)(μ<sub>3</sub>-O<sub>4</sub>)(μ<sub>4</sub>-O<sub>4</sub>)(NH<sub>3</sub>)<sub>32</sub>](NO<sub>3</sub>)<sub>8</sub>·19.6 NH<sub>3</sub> – the Largest Thorium Complex from Solution known to Date. *Zeitschrift für anorganische und allgemeine Chemie* **2014**, *640* (8–9), 1547–1550.

(42) Albrecht, A. J.; Sigmon, G. E.; Moore-Shay, L.; Wei, R.; Dawes, C.; Szymanowski, J.; Burns, P. C. The crystal chemistry of four thorium sulfates. *J. Solid State Chem.* **2011**, *184* (7), 1591–1597.

(43) Knopf, K. E.; Soderholm, L. Solution and Solid-State Structural Chemistry of Actinide Hydrates and Their Hydrolysis and Condensation Products. *Chem. Rev.* **2013**, *113* (2), 944–994.

(44) Kalaji, A.; Skanthakumar, S.; Kanatzidis, M. G.; Mitchell, J. F.; Soderholm, L. Changing Hafnium Speciation in Aqueous Sulfate Solutions: A High-Energy X-ray Scattering Study. *Inorg. Chem.* **2014**, *53* (12), 6321–6328.

(45) Kalaji, A.; Soderholm, L. Aqueous Hafnium Sulfate Chemistry: Structures of Crystalline Precipitates. *Inorg. Chem.* **2014**, *53* (20), 11252–11260.

(46) Ruther, R. E.; Baker, B. M.; Son, J.-H.; Casey, W. H.; Nyman, M. Hafnium Sulfate Prenucleation Clusters and the Hf<sub>18</sub> Polyoxometalate Red Herring. *Inorg. Chem.* **2014**, *53* (8), 4234–4242.

(47) Sigmon, G. E.; Burns, P. C. Rapid Self-Assembly of Uranyl Polyhedra into Crown Clusters. *J. Am. Chem. Soc.* **2011**, *133* (24), 9137–9139.

(48) Shannon, R. Revised effective ionic radii and systematic studies of interatomic distances in halides and chalcogenides. *Acta Crystallogr., Sect. A* **1976**, *32* (5), 751–767.

(49) SAINT Plus, version 8.34a; Bruker AXS Inc.: Madison, WI, 2013.

(50) Sheldrick, G. M. SADABS: *Bruker/Siemens Area Detector Absorption Correction Program*, version 2008/12008; Bruker AXS Inc.: Madison, WI, 2008.

(51) Sheldrick, G. M. SHELXT - Integrated space-group and crystal-structure determination. *Acta crystallographica section A: Foundations and Advances* **2015**, *A71*, 3–8.

(52) Sheldrick, G. M. A short history of SHELX. *Acta Crystallogr., Sect. A: Found. Crystallogr.* **2008**, *64* (1), 112–122.

(53) Dolomanov, O. V.; Bourhis, L. J.; Gildea, R. J.; Howard, J. A.; Puschmann, H. OLEX2: a complete structure solution, refinement and analysis program. *Journal of applied crystallography* **2009**, *42* (2), 339–341.

(54) Ilavsky, J.; Jemian, P. R. Irena: tool suite for modeling and analysis of small-angle scattering. *J. Appl. Crystallogr.* **2009**, *42*, 347–353.

(55) Zuo, X.; Cui, G.; Merz, K. M.; Zhang, L.; Lewis, F. D.; Tiede, D. M. X-ray diffraction “fingerprinting” of DNA structure in solution for quantitative evaluation of molecular dynamics simulation. *P Natl. Acad. Sci. USA* **2006**, *103*, 3534–3539.

(56) Estes, S. L.; Antonio, M. R.; Soderholm, L. Tetravalent Ce in the Nitrate-Decorated Hexanuclear Cluster [Ce<sub>6</sub>(μ<sub>3</sub>-O)<sub>4</sub>(μ<sub>3</sub>-OH)<sub>4</sub>]<sub>12</sub><sup>+</sup>: A Structural End Point for Ceria Nanoparticles. *J. Phys. Chem. C* **2016**, *120* (10), 5810–5818.